Climatic Change (2025) 178:111
https://doi.org/10.1007/s10584-025-03951-2

High-resolution projection of wind energy in the Eastern Mediterranean and Middle East summer

Melissa Latt[1] · **Marianna Adinolfi**[2] · **Paola Mercogliano**[2] · **Assaf Hochman**[3]

Received: 17 June 2024 / Accepted: 8 May 2025 / Published online: 23 May 2025

Abstract

Understanding the impacts of climate change on wind patterns and wind power potential is crucial for energy planning and resource management, particularly in regions highly vulnerable to climate variability, such as the Middle East. In this study, we used COSMO-CLM regional climate model simulations at $8\,\mathrm{km}$ grid spacing to analyze summer wind pattern changes in the Middle East and their impact on the wind energy potential. Our analysis reveals that COSMO-CLM can effectively capture broad-scale summer wind patterns in the Middle East. However, considerable uncertainties were observed in coastal and mountain regions, highlighting the complexity of local wind dynamics. In particular, until 2070, we identified significant increases of up to $0.7\,\mathrm{ms}^{-1}$ in median surface wind speeds throughout the Middle East, driven primarily by land-sea temperature contrasts. However, at the 150-meter level, we project significant decreases of up to $1.0\,\mathrm{ms}^{-1}$ in the median wind speed attributed to changes in the frequency and intensity of the Persian Trough synoptic system in a changing climate. Regionally, this reduces the median potential wind energy by up to 7 GJ in six hours. These findings underscore the importance of considering surface and upper-level wind characteristics when assessing the impacts of climate change on wind energy resources. Furthermore, our study reveals a spatially heterogeneous pattern of changes in the wind energy potential throughout the region. Although decreases in wind energy are evident throughout the Middle East, particularly in inland areas and over the Mediterranean Sea, we also observe some increases in potential, notably over the Red Sea. In summary, our study highlights significant changes in wind characteristics in a changing climate, with implications for the future energy mix in the Middle East. These findings provide valuable information for policy-makers and energy planners aiming to sustainably harness wind energy resources in the face of climate change challenges.

Highlights

- COSMO-CLM captures summer wind patterns but struggles in coastal, hilly areas.
- Surface winds are projected to increase by 0.7 ms^{-1}, and 150 m winds are projected to decrease by 1.0 ms^{-1} in the Middle East by 2070.
- Upper wind changes cut potential energy by 7 GJ $6h^{-1}$; increase in potential energy on the red sea.

Extended author information available on the last page of the article

- This study emphasizes the consideration of surface and upper winds for the impact of climate on energy.
- Spatial wind energy changes in the Middle East impact sustainable energy planning.

Keywords Eastern Mediterranean · Wind power · Renewable energy · Climate change · Downscaling · Climate impacts

1 Introduction

The extreme summer heat in the Middle East creates significant challenges for society because of the threat of heat stress (Hochman et al. 2022; Zittis et al. 2022; Wedler et al. 2023). Despite this severe climate, winds are a natural mechanism for alleviating intense heat. The interplay between regional topography, land-sea temperature differences, and broader atmospheric circulation patterns shapes the dynamics of summer winds in the Middle East, influencing their ability to mitigate heat stress (Ziv et al. 2004). By promoting evaporative cooling and dispersing heat, winds play a vital role in lowering local temperatures and mitigating the harmful effects of extreme heat on human health and well-being (Lee et al. 2018; Åström et al. 2011; Chen et al. 2015).

Understanding and predicting summer winds in the Middle East is important for more than addressing heat stress, as they hold critical importance for the development of renewable energy, particularly wind power (Pryor et al. 2020; Gernaat et al. 2021; Kiriakidis et al. 2024). Examining how climate change-induced variations could influence the efficiency and structural integrity of energy sources and facilities is essential for advancing renewable technologies and aiding communities, designers, and policy-makers (Adinolfi et al. 2020). With a rapidly expanding population and increasing energy needs, diversifying energy sources and reducing fossil fuel dependence are urgent priorities (Sadorsky 2021). The Middle East, which is rich in oil and natural gas, has seen growing investment in wind energy. Large wind farms have existed in Iran for 15 years, and significant new projects have been carried out in recent years (Kharat Halou 2012). Notable wind farms include the 400 MW Dumat Al-Jandal in Saudi Arabia (Imam et al. 2024), the 200 MW Genesis project in Israel's Golan Heights (Eitan and Fischhendler 2023), a 29 MW plant near Nishapur, Iran (Katal and Fazelpour 2018), the 117 MW Tafila wind farm in Jordan (Holtz and Fink 2015), and the 260 MW Ras Ghareb farm on Egypt's Red Sea coast (Hamdi et al. 2023). Expansion plans include Saudi Arabia's goal of 9.5 GW of renewable energy by 2030 (Amran et al. 2020) and the 250 MW North Ras Gharib project near the Gulf of Suez, Egypt (Serckx et al. 2018). Wind energy presents a viable solution due to its abundance and sustainable nature (Hassan et al. 2023). The significant wind energy potential of the region highlights the need for precise wind projections to identify optimal locations for wind farms and maximize energy output (Chen et al. 2018). By harnessing wind energy, the Middle East can diversify its energy mix, decrease fossil fuel reliance, and contribute to global climate change mitigation efforts (Hassan et al. 2023). Thus, studying summer winds in the Middle East has dual objectives: guiding heat stress mitigation strategies to safeguard public health and enabling the sustainable development of wind energy resources to meet increasing energy demands while increasing the climate resilience and environmental sustainability of the region.

The Middle East, renowned for its hot and arid summer climate, offers a dynamic setting for wind projections influenced by numerous climatic factors (Ziv et al. 2004; Harpaz et al. 2014; Hochman et al. 2021). The summer months of the region are marked by high temperatures and dry landscapes, creating complex interactions of atmospheric dynamics that significantly influence wind patterns (Hochman et al. 2022; Latt et al. 2022). Key regional weather systems, such as the subtropical high and the Persian Trough, play crucial roles in shaping these prevailing winds (Alpert et al. 2004a, b; Hochman et al. 2018b, c; Alpert et al. 1990). These atmospheric systems create diverse wind regimes across different terrains, from coastal areas to vast deserts and rugged mountains (Ziv et al. 2004; Saaroni et al. 2017). Additionally, the summer climate of the region is characterized by frequent dust storms, further complicating wind dynamics (Rezazadeh et al. 2013; Crouvi et al. 2017; Baltaci 2021; Gasch et al. 2017). Strong diurnal temperature variations and the development of thermal low-pressure systems contribute to localized wind patterns, such as sea breezes and mountain–valley winds (Kunin et al. 2019; Latt et al. 2022; El-Geziry et al. 2021). Integrating these climatic details into high-resolution models is essential for maximizing the wind energy potential of the region (Latt et al. 2022).

Accurate global and regional wind energy potential projections are critical for advancing renewable energy initiatives and addressing heat stress (Jung and Schindler 2022). This task necessitates advanced modeling techniques such as dynamical downscaling. Regional circulation models (RCMs) (Tapiador et al. 2020; Hochman et al. 2018a; Krichak et al. 2010) provide a detailed depiction of atmospheric circulation at fine spatial resolutions, allowing for a comprehensive analysis of local-scale features crucial for precise wind assessments (Latt et al. 2022; Kulkarni et al. 2019; Reale et al. 2022; Molina et al. 2024). RCMs enhance coarse-scale global circulation models (GCMs) by incorporating high-resolution topographic and land-use data, thus more accurately capturing site-specific conditions (Giorgi et al. 2009; Giorgi and Gutowski 2015). In the Middle East, with its varied terrain and climatic interactions, the application of RCMs is particularly valuable (Hochman et al. 2018a; Latt et al. 2022; Chen et al. 2018; Gasch et al. 2017). This approach offers a detailed understanding of regional atmospheric dynamics, including the effects of topography on wind flow patterns and the impact of local land surface characteristics on wind modulation (Latt et al. 2022).

Several studies have revealed a troubling predicted scenario of extreme heatwaves and extended droughts in the region (Zittis et al. 2022; Hochman et al. 2022). Temperatures are expected to rise significantly above current levels, worsening water scarcity and placing tremendous pressure on agricultural productivity, urban infrastructure, and public health (Samuels et al. 2018; Wedler et al. 2023). Coastal areas are particularly vulnerable and face increased risks of heat-related illnesses, high humidity, and the additional challenge of rising sea levels. Despite this, investigations into wind systems in the region have been limited, with only a few studies addressing this topic (Kunin et al. 2019; Chen et al. 2018; Alpert and Getenio 1988). These studies have mostly utilized coarse climate model simulations or high-resolution applications focused on specific case studies (Kunin et al. 2019; Shafir et al. 2008; Kishcha et al. 2018; Kiriakidis et al. 2024; Gasch et al. 2017). More recently, Latt et al. (2022) explored the simulation of key summer wind systems in Israel via the COSMO-CLM model with "perfect" boundary conditions from the ERA5 reanalysis (see Sect. 2.2). Their findings have indicated that a grid spacing finer than 10 km is necessary to accurately capture the interactions between mesoscale wind features, such as Mediterranean

Sea breezes and mountain–valley winds, and synoptic-scale influences, such as the Persian Trough and the subtropical high.

We aim to project climate change-induced shifts in summer wind fields across the Middle East, both near the surface and at 150 m (wind turbine height). Therefore, we use high-resolution (8 km) COSMO-CLM simulations with a 6 hourly time resolution under the IPCC RCP4.5 scenario up to 2070 within the CORDEX-MENA domain. To validate the climate simulations, the results under current climate are compared with three reanalysis products. Afterwards, anomalies are assessed as the difference between future projections and past climate. The article is organized as follows: Section 2 describes the data used for evaluation, the overall model setup and the statistical inference methodology. The results are presented in three sections: first, an evaluation of the model concerning various reanalysis and observational products (Section 3.1) and then projections of wind (Section 3.2) and potential wind energy (Section 3.3) are performed. Section 4 provides a summary and concluding remarks.

2 Data and methods

2.1 Data

The wind and surface temperature data used in this study encompassed atmospheric reanalysis datasets, including ERA-Interim (Dee et al. 2011), ERA5-Land (Muñoz Sabater 2019), and UERRA (Copernicus Climate Change Service 2019) datasets. ERA-Interim, produced by the European Centre for Medium-Range Weather Forecasts (ECMWF), is widely recognized for its comprehensive coverage and reliability, spanning from 1979 to 2019, with a spatial resolution of approximately 0.75 degrees (Dee et al. 2011). ERA5-Land, a newer iteration released by ECMWF, builds upon its predecessor by incorporating land-specific variables with a higher spatial and temporal resolution (approximately 0.1 degrees and hourly) and an improved representation of surface processes, extending from 1950 to the present (Muñoz-Sabater et al. 2021). Uncertainties in Ensembles of Regional Reanalyses (UERRA), was developed through collaborative efforts and complements these global datasets with a focus on regional scales, offering valuable insights into localized climatic phenomena and uncertainties over Europe and the Eastern Mediterranean. We used UERRA (MESCAN-SURFEX option), a reanalysis at approximately 5.5 km, which provides estimations of the climate from 1961 to 2019. It combines the MESCAN system and the land surface platform SURFEX with UERRA-HARMONIE reanalysis (approximately 11 km) and additional surface observations to switch on more advanced physics options for better representing surface variables and soil processes at a 6-hourly temporal resolution. UERRA-HARMONIE is based on a 3-D data assimilation system assumed from the lateral border data from ERA40 (Uppala et al. 2005) before 1979 and ERA-Interim until 2019. While ERA-Interim and ERA5-Land and provide a global perspective, UERRA offers finer details at the regional level, aiding in understanding sub-regional climate dynamics and variability (Kaiser-Weiss et al. 2019).

2.2 Model setup

We utilized the COSMO-CLM regional climate model (Rockel et al. 2008), which is an adaptation of the COSMO-LM mesoscale weather forecast model (Steppeler et al. 2003), for two simulations within the CORDEX-MENA domain (27 ° −76 °E, 7 °S −45 °N) (Giorgi et al. 2009) and further downscaling, nested in the previous runs, at approximately 8 km ($0.075\,^{\circ}$) in a reduced domain. The former simulations in the CORDEX-MENA domain, conducted at resolutions of approximately 50 km (0.44 °) and 25 km (0.22 °), used an optimized configuration developed through extensive sensitivity analyses (Bucchignani et al. 2016a). The configuration includes parameterizations for surface albedo based on MODIS data (Lawrence and Chase 2007), the NASA-GISS aerosol optical depth distribution (Tegen et al. 1997), and the Tiedtke cumulus convection scheme (Tiedtke 1989). The model domain features a relaxation area extending 15 grid points from each boundary, with the initial year of simulation, i.e., 1979, serving as a spin-up period and thus excluded from analysis. The evaluation run was driven by ERA-Interim reanalyses. Future climate projections under the IPCC RCP4.5 scenario, which assumes that greenhouse gas concentrations will peak at approximately 2040 before declining (Moss et al. 2010), were performed using initial and boundary conditions from the CMCC-CM global climate model (GCM) (Scoccimarro et al. 2011). The IPCC RCP4.5 scenario represents a medium stabilization pathway, where radiative forcing is stabilized at $4.5\,\mathrm{W/m^{-2}}$ by the year 2100. Given that the RCP4.5 and other RCP scenarios diverge in the middle of the century and that this study focuses on that period for practical reasons, only RCP4.5 is adopted to reduce the computational burden associated with dynamical downscaling. The new high-resolution simulation at approximately 8 km ($0.075\,^{\circ}$) grid spacing and 6-hourly temporal resolution, nested into the one at approximately 25 km grid spacing (Bucchignani et al. 2018, 201b6), covers a limited domain (28.10 °E−39.45 °E, 24.01 °N−35.45 °N). A third-order Runge–Kutta scheme was employed for time integration, with the atmospheric model comprising 40 vertical levels and seven soil levels. The evaluation period spans from 1981 to 2010, with projected climate changes assessed from 1981 to 2070.

2.3 Methods for model evaluation, climate projection, and potential wind energy calculation

The performance of the COSMO-CLM model in reproducing wind characteristics over the study domain is evaluated by focusing on the summer months (July and August), when thermal wind systems dominate alongside the Persian Trough and subtropical high, with minimal synoptic-scale disturbances (Naor et al. 2017).

For validation, the COSMO-CLM simulation is compared with reanalysis datasets (see Section 2.1) by analyzing the spatial distribution of near-surface wind speeds over a 30-year period (1981–2010) at four daily time steps (00, 06, 12, and 18 UTC). Differences between COSMO-CLM outputs and reanalysis products were assessed via the nearest-neighbor interpolation method, which aligns model outputs with the coarser reanalysis grid.

For climate change projections, the spatial distributions of near-surface and 150 m wind speeds are analyzed alongside the near-surface temperature. Statistical significance is assessed via the Wilcoxon rank-sum test at the 5 % level (Wilcoxon et al. 1970).

To evaluate the impact of climate change on wind energy potential, specific regions within the study domain (Fig. 1), including the Red Sea (RS), Golan Heights (GH), Mediterranean Sea Coast (MSC), Nile Delta (ND), Plain (PL), Mediterranean Sea (MS), Judean Mountains (JM), and Sinai Peninsula (PS), are statistically analyzed.

Finally, the theoretical wind energy (E_W) and effective wind energy potential per wind turbine (E_{WT}) are computed (Adekoya and Adewale 1992):

$$\begin{aligned} E_W &= 0.5\pi r^2 \rho v^3 t \\ E_{WT} &= \eta E_W \end{aligned}$$

We assume that the radius of the rotator blades is $r = 40\,\mathrm{m}$ and that the density of air is $\rho = 1.18 kg/m^3$. E_{WT} is the effective wind energy potential for a wind turbine remaining from the theoretical wind energy E_W considering its efficiency, which we assume is $\eta = 40\,\%$. Finally, we use a time reference matching the temporal resolution of the COSMO-CLM model of six hours $t = 21600\,\mathrm{s}$.

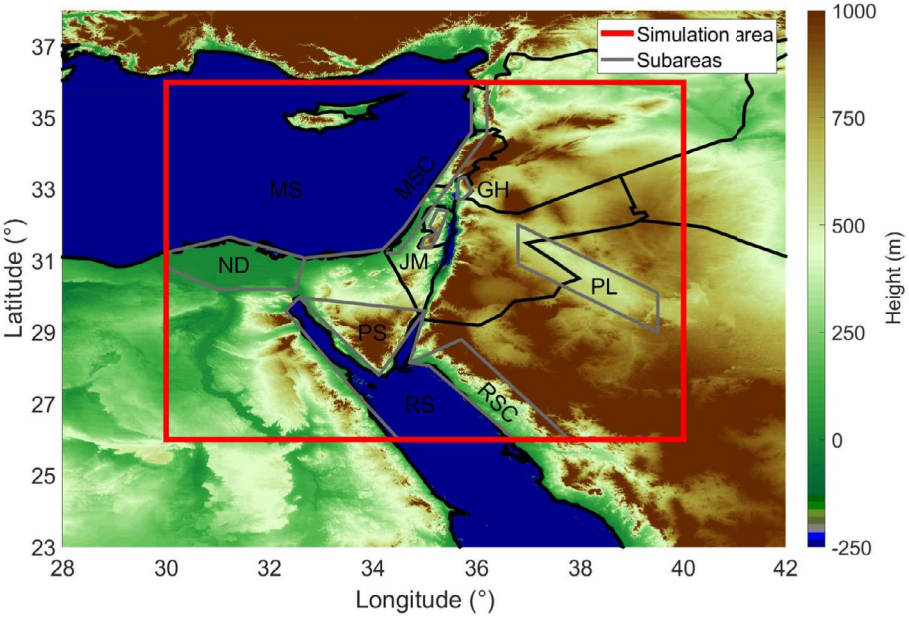

Fig. 1 Simulation area of the COSMO-CLM simulation at $\Delta x \approx 8\,\mathrm{km}$ grid spacing. The vertices of the red simulation area are located at 26.01 °N, 30.01 °E and 35.59 °N, 39.59 °E. The gray areas represent subareas that are referred to in further analyses: the Nile Delta (ND), Mediterranean Sea (MS), Mediterranean Sea Coast (MSC), Judean Mountain (JM), Sinai Peninsula (PS), Golan Heights (GH), Plain (PL), and Read Sea Coast (RSC)

3 Results

3.1 Evaluation of the 8 km COSMO-CLM model simulation

First, we evaluate the ability of COSMO-CLM to capture the main wind systems over the Middle East during summer. A comprehensive evaluation of the same model with the same setup is given in Latt et al. (2022) and Hochman et al. (2018a). Here, we extend the evaluation for selected wind variables relevant to the wind energy potential. Figure 2 shows the 10

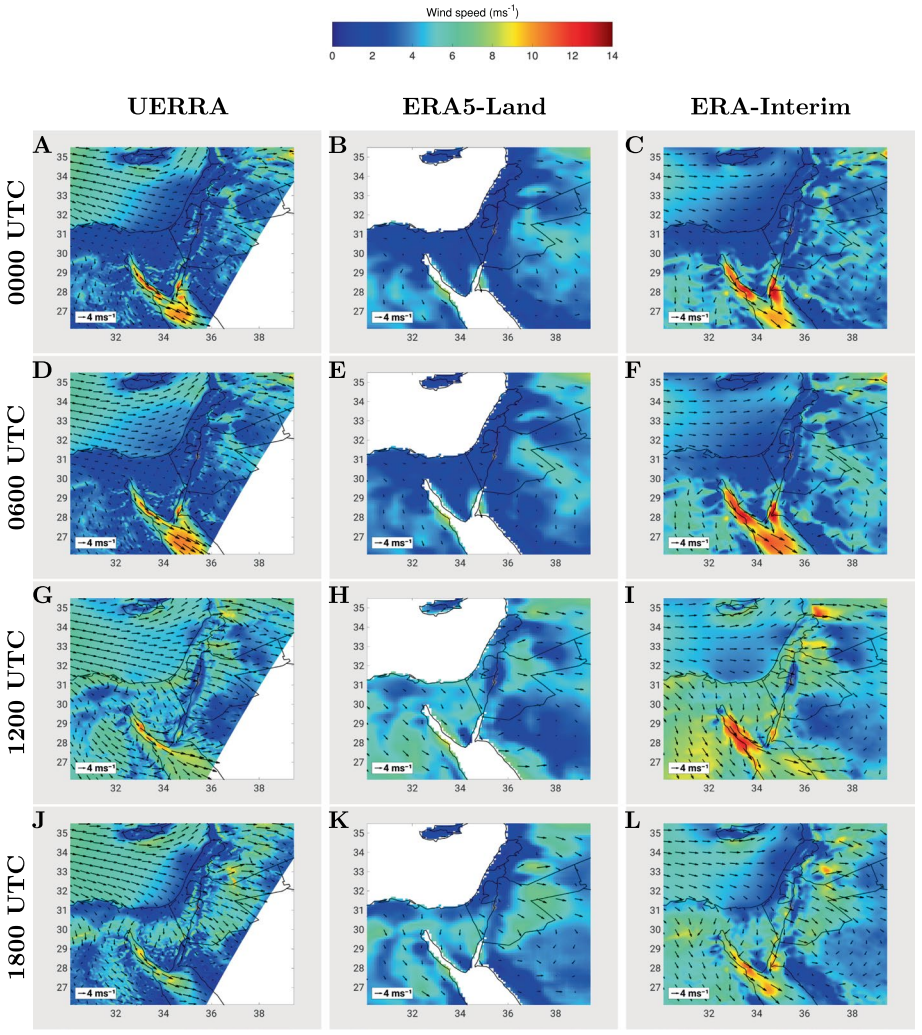

Fig. 2 Summer (July and August) median (1981–2010) of modeled near-surface wind fields for the reanalysis UERRA (**a**, **d**, **g**, **j**), ERA5-LAND (**b**, **e**, **h**, **k**) and ERA-Interim (**c**, **f**, **i**, **l**) at 0000 UTC (**a**, **b**, **c**), 0600 UTC (**d**, **e**, **f**), 1200 UTC (**g**, **h**, **i**) and 1800 UTC (**j**, **k**, **l**). The UERRA data were only available for 1985–2010. The axes indicate latitude and longitude in degrees north and east, respectively. The wind speed is represented by colors, and the wind direction is represented by arrows scaled with the wind speed

m wind median summer climatology for 1981–2010, the 10 m wind direction and the wind speed for the different reanalysis products and four times daily.

During the night and early morning (Fig. 2a, b, c, d, e, f), the wind speeds are predominantly low over land (up to 6 ms^{-1}). UERRA reanalyses reveal weak westerly winds blowing in the coastal area of the Mediterranean Sea. The Red Sea is affected by the highest wind speeds (up to 14 ms^{-1}) in the North–South direction, as reported by both UERRA and ERA-Interim due to the tunneling effect of the Jordan Valley (Langodan et al. 2017). During the day and in the late afternoon (Fig. 2g, h, i, j, k, l), the wind speed slightly increased over land over the Sinai Peninsula and decreased over the Red Sea compared with that in the nighttime and early morning. The increases over land are more pronounced in the ERA-Interim reanalyses (up to 10 ms^{-1} at 1200 UTC), although they are confirmed over inland territories by UERRA and ERA5-Land (up to 9 ms^{-1}). The strongest wind speeds of up to 13 ms^{-1} are simulated from northwesterly to northeasterly directions in the northern area of the Red Sea, especially at night and in the early morning; this holds true across all reanalysis products and times of day. The Mediterranean Sea breeze, a persistent wind system in the Middle East summer peaks in the afternoon (Kunin et al. 2019). ERA5 Land cannot capture the sea breeze over the Mediterranean Sea and its coasts, in agreement with Latt et al. (2022). UERRA and ERA-Interim can reproduce the sea breeze quite well.

Next, to highlight the potential and limitations of the model used, we present the differences between our 8 km COSMO-CLM simulation and various reanalysis datasets (Fig. 3). When comparing COSMO-CLM, CERRA, and ERA5, it should be noted that COSMO-CLM, UERRA, and ERA5 have different spatial and temporal model resolutions, which can lead to uncertainties (Nolan et al. 2014). The models can capture the high natural spatial and temporal variability of wind fields in different detail. COSMO-CLM overestimates wind speeds mainly over the Red Sea and its coasts, the Sinai Peninsula, and the Nile Delta (bias up to 6 ms^{-1}). Coastal areas are often characterized by complex orography that models with a coarse resolution cannot capture. Latt et al. (2022) reported that wind speeds are underestimated by ERA5, especially in coastal or orographically complex areas. Therefore, the underestimation of the wind speed by ERA5 in complex areas, among other things, result in the large positive differences between the COSMO and ERA5 wind speeds. Another effect causing positive wind speed bias could be that the COSMO-CLM surface drag near the coast is too low (Nolan et al. 2014). Compared with UERRA (Fig. 3a, d, g, j), however, it provides good performance along the Mediterranean coasts (bias up to 2 ms^{-1}). COSMO-CLM overestimates wind speeds mainly along the Mediterranean coasts and the Sinai Peninsula (with bias up to 6 ms^{-1} at 1200 UTC) and largely provides good performance elsewhere (bias up to 2 ms^{-1}) compared with ERA5-Land (Fig. 3b, e, h, and k). COSMO-CLM underestimates wind speeds along the Mediterranean Sea, Red Sea, and Golan Heights and Plains (with bias up to -1 ms^{-1}), and it provides diffuse overestimation (bias up to 1 ms^{-1} at 1200 UTC) compared with ERA-Interim (Fig. 3c,f, i, l). The biases between COSMO-CLM and UERRA are generally lower than those between COSMO-CLM and ERA5, as verified over different areas and resolutions (Adinolfi et al. 2023). Although non-negligible biases in wind speeds and directions are simulated by COSMO-CLM compared with reanalysis products, overall, it is evident that COSMO-CLM can reproduce local wind patterns, even in complex geographical locations of the domain, close to the mid-latitude and subtropical zones. Moreover, the uncertainties in the regional climate model and reanalysis products associated with the limitations of the adopted parameterizations and forcing data, as do the

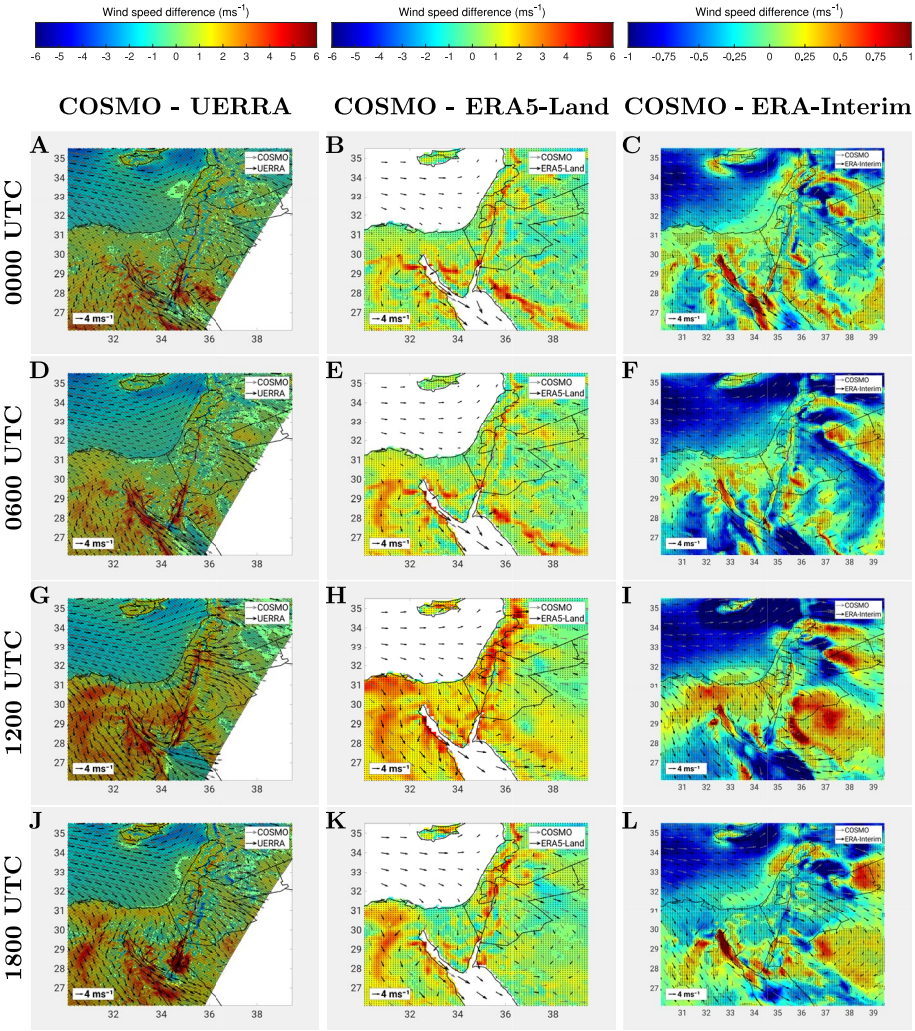

Fig. 3 Summer (July and August) median (1981–2010) differences in modeled COSMO near-surface wind fields and UERRA reanalysis (**a**, **d**, **g**, **j**), ERA5-LAND (**b**, **e**, **h**, **k**), ERA-Interim (**c**, **f**, **i**, **l**) at 0000 UTC (**a**, **b**, **c**), 0600 UTC (**d**, **e**, **f**), 1200 UTC (**g**, **h**, **i**), and 1800 UTC (**j**, **k**, **l**). The UERRA data were only available for 1985–2010. The small black dots indicate if the difference is significant (Wilcoxon rank sum test at the 5 % significance level). The axes indicate latitude and longitude in degrees north and east, respectively. The wind speed is represented by color, and the wind direction is represented by arrows scaled with the wind speed

GCM and coarse resolution simulations, should be considered. The COSMO-CLM model is not coupled over seas and oceans. This limitation affects the performance of the atmospheric variables over coastal areas and islands (Iglesias et al. 2023). In contrast, we should consider the limited availability of observations over Africa, where reanalysis mainly results from the driving model rather than from observations. We, therefore, practically compare the model to the model in those regions. These aspects probably explain the larger biases found over Africa than over Israel, where more observations are available. In summary, although we

find some biases over coastal and mountainous regions, the 8 km COSMO-CLM simulation can largely mimic summer wind patterns over the Middle East and, therefore, may be used for climate change projections.

3.2 Projection of near-surface wind

Climate change is expected to significantly increase the already high summer temperatures in the Eastern Mediterranean and Middle East. Near-surface winds are a natural mechanism for reducing heat stress (see Sect. 1). In the following, the COSMO-CLM near-surface winds are compared between 1981 and 2010 and between 2041 and 2070 to describe changes in the wind field with increased greenhouse gas concentrations and link them to near-surface temperature development.

The wind speeds are predominantly low during the night and in the early morning (Fig. 4a, b, d, e). Weak westerly winds of up to 2 ms^{-1} blow in the coastal area of the Mediterranean Sea. Only small, insignificant changes in wind speed are expected on the coast at these times of day until 2070 under the RCP4.5 scenario (Fig. 4c, f). Surface temperatures rise almost uniformly for the Mediterranean Sea by $1.5\,°$. In coastal areas, the temperature increases up to $2.0\,°$(Fig. 5c, f). There is a consensus that the temperature in the eastern Mediterranean will increase with climate change. The extent of the simulated temperature increase depends on the emission scenario selected, the period considered, and the model used. Various studies project summer temperature increases of 3 to 7 degrees Celsius in the eastern Mediterranean by the end of the century (Lelieveld et al. 2014; Zittis et al. 2016; Evans 2009; Giorgi and Lionello 2008). The Red Sea and Mediterranean coastal areas are simulated to be the regions with the smallest rise in temperature, at $1.5\,°$. The nocturnal land wind cannot be identified. This is because the maximum amplitude of the onshore wind may not be captured at a temporal resolution of 6 hours. A steady westerly wind with speeds of approximately 4 ms^{-1} blows over the Mediterranean, which turns to the southwest east of Cyprus and to the northwest north of the Egyptian coastline. Small increases in wind speed are expected in this area, but these increases are insignificant (Fig. 4c, f). The wind reaches speeds of approximately 5 ms^{-1}(Fig. 4a, b, d, e) further inland in areas at higher altitudes, such as the Judean Mountains, the Jordanian Mountains, and the Nafud Desert. The wind is weaker in the valleys, with speeds of approximately 2 ms^{-1}. Especially on the northern and western edges of the Nafud Desert, the northeasterly to northwesterly winds are projected to increase by 0.4 ms^{-1}. The warm desert will warm faster than the surrounding regions, which increases the temperature gradient and, hence, the thermal circulation (Fig. 5c, f). West of the Red Sea, the wind comes from northerly directions with 3 ms^{-1} to 5 ms^{-1}(Fig. 4a, b, d, e). The cooler coastal part north of the Nile Delta warms slower than does the southern part of the Delta, increasing temperature gradients and significantly increasing the median wind velocity to 0.6 ms^{-1}. On the east coast of the Red Sea, weak winds blow from the northeast, which are projected to decrease even more in the future. The same applies to parts of the west coast. These regions are warmer at night than the surrounding areas are (Fig. 5a, d). According to the simulation, the warm coast of the Red Sea will experience a smaller temperature increase in the future than the surrounding land areas (Fig. 5c, f). This reduces the nighttime temperature gradient and, therefore, the land wind intensity. In contrast, the median wind speed of the weak winds along the Dead Sea Valley are projected to increase by up to 0.3 ms^{-1}. At all four times of day, the highest wind speeds of up to 13

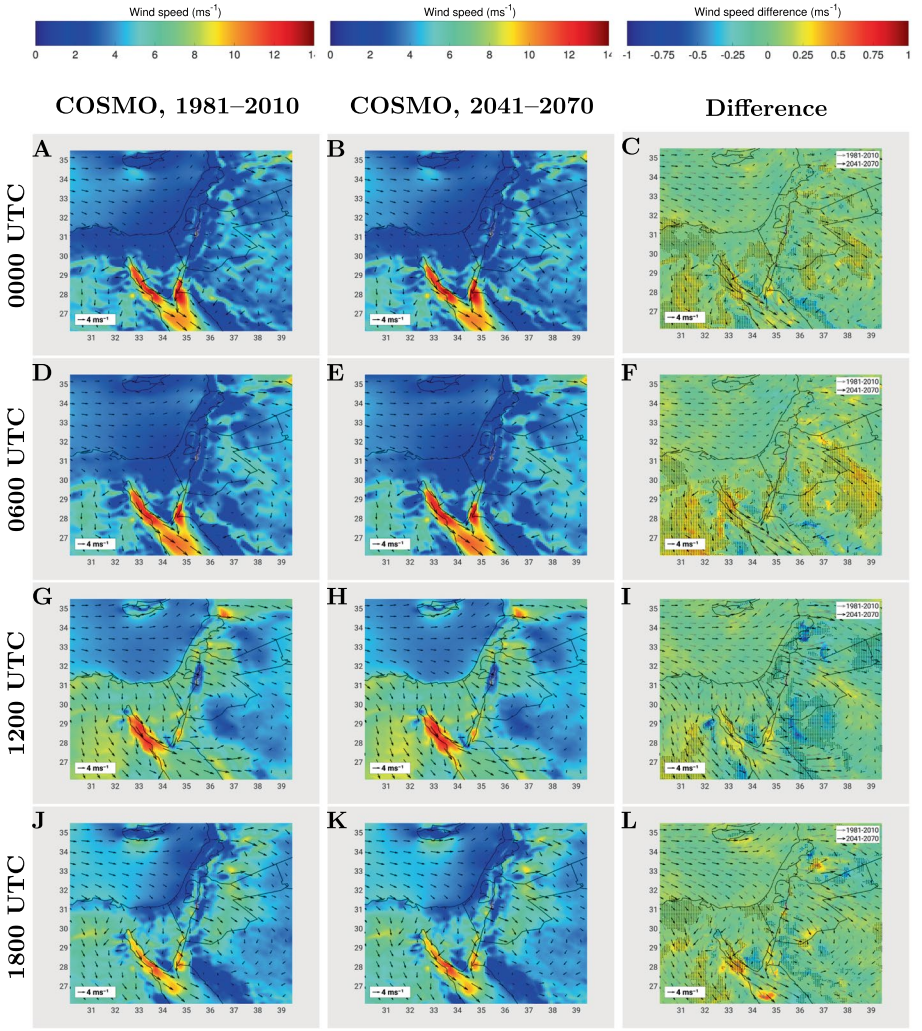

Fig. 4 Summer (July and August) median of simulated COSMO-CLM near-surface wind fields averaged over the time periods 1981–2010 (**a**, **d**, **g**, **j**), 2041–2070 (**b**, **e**, **h**, **k**), and their differences (2041–2070 - 1981–2010) (**c**, **f**, **i**, **l**) at 0000 UTC (**a**, **b**, **c**), 0600 UTC (**d**, **e**, **f**), 1200 UTC (**g**, **h**, **i**), and 1800 UTC (**j**, **k**, **l**). The black dots indicate whether the difference is significant on the basis of a Wilcoxon rank-sum test at the 5 % significance level. The axes indicate latitude and longitude in degrees north and east, respectively. The wind speed is represented by colors, and the wind direction is represented by arrows scaled with the wind speed

ms^{-1} are simulated from northwesterly to north-easterly directions in the northern area of the Red Sea. Particularly in the northwestern arm of the Red Sea, a further increase in the median wind speeds of up to 0.5 ms^{-1} of the already high wind speeds is projected at all times of the day.

At 1200 UTC (Fig. 4g, h), the wind speeds over land reach their maximum values because of thermal wind systems, which are driven by large local temperature differences (Fig. 5g, h). The Mediterranean Sea breeze blows at approximately 8 ms^{-1} near the coast.

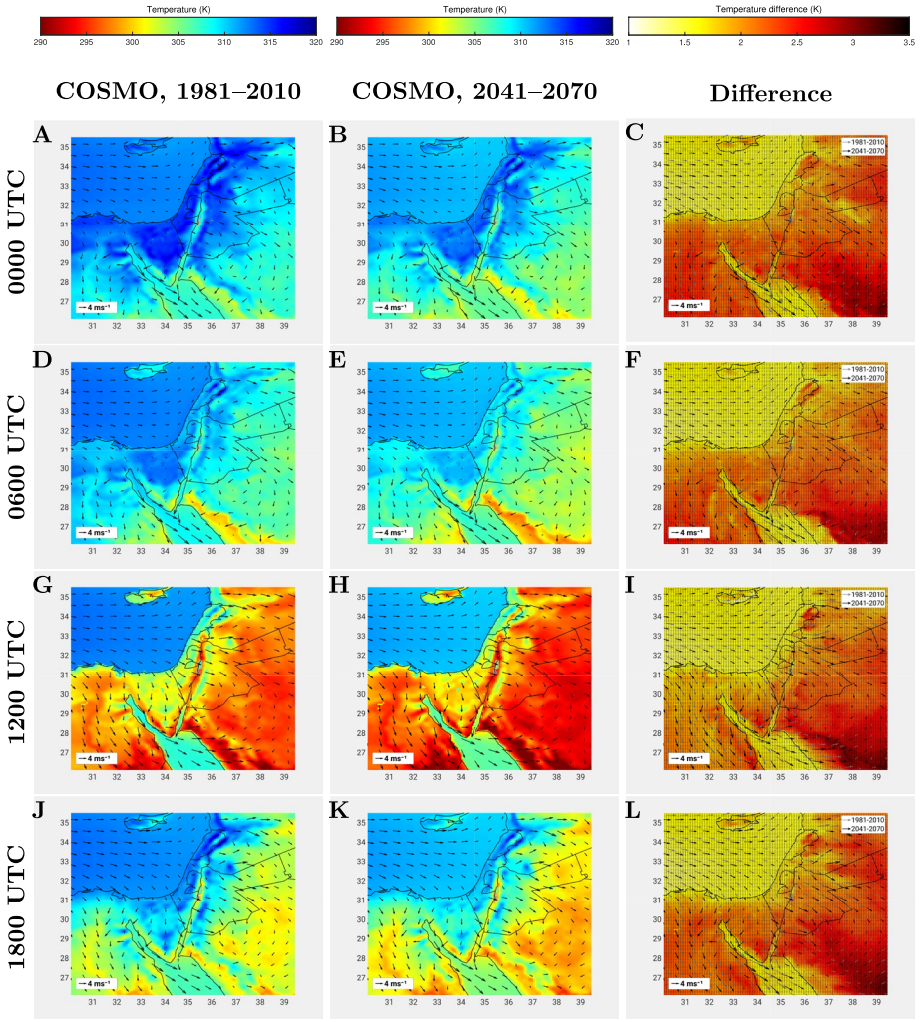

Fig. 5 The same as in Fig. 4, but the colors represent the near-surface temperature

Further inland, this area overlaps with the upslope winds of the Judea Mountains (Latt et al. 2022). Wind speeds in the southern Jordanian Mountains are expected to decrease by a median of 0.3 ms^{-1} by 2070 (Fig. 4i). Similar behavior can be observed in the western hills of the Red Sea. The upslope winds in the Jordanian Mountains provide northwesterly winds with speeds of up to 9 ms^{-1}. No statistically significant changes in the wind speed or direction are projected there. Over the Mediterranean Sea, a steady wind arrives from westerly directions with speeds of 4 ms^{-1}. Again, no significant change in wind speed over the Mediterranean Sea is projected. In the Red Sea, the sea breeze blows at speeds of 9 ms^{-1}. On the east coast, the sea breeze slows the warming of the surface. Therefore, the temperature gradient between the Red Sea and the coast does not change much (Fig. 5g, h, i). At the Red Sea coastline, the median decrease in wind speed is 0.3 ms^{-1}(Fig. 4i). At 1200 UTC, the area with decreasing near-surface wind speeds was the largest compared with the

other times of day (Fig. 4i). North of the Golan Heights, in the Syrian Desert, Judean and Jordanian Mountains, parts of the Red Sea coast, and in the northwestern area of the Nafud Desert, decreases in the median wind speeds of 0.2 ms^{-1} to 0.5 ms^{-1} are projected. Nevertheless, significant increases in wind speed are projected south of the Nile Delta and in the northwestern area of the Red Sea.

Toward the evening, the temperature gradients decrease (Fig. 5j, k), and the thermal wind systems and thus the wind speeds weaken in most regions (Fig. 4j, k). However, the wind directions hardly change compared with those at 12 UTC. While westerly winds with speeds of 5 ms^{-1} are simulated over the Mediterranean Sea, the winds on the coasts of the Mediterranean and the Dead Sea only reach 2 ms^{-1} as the sea breeze almost vanishs. The upslope winds further west, strengthened by the sea breeze, last longer in the evening than the sea breeze near the shore, so that wind speeds of 8 ms^{-1} are still achieved locally over the Judean and Jordanian Mountains. Over the northern part of the Red Sea, in the Nile Delta and to its south, the wind speed reaches 5 ms^{-1} to 12 ms^{-1}(Fig. 4j, k). For these regions, the median wind speed is projected to increase by 0.1 ms^{-1} to 0.5 ms^{-1} by 2070 (Fig. 4l). On the east coast and a part of the north coast of the Red Sea, in the northwestern part of the Nafud Desert, and in northeastern Jordan, a decrease in wind speed is projected.

Overall, future changes in the near-surface wind over the Middle East are determined mainly by changes in the near-surface temperature gradients, as the wind field is dominated on most summer days by thermal wind systems such as land–sea wind circulation, valley winds, and slope winds. An increase in wind speed is projected for most regions and at most times of the day, which can moderate the increasing heat stress caused by climate change. The highest increases in the median wind speed of up to 0.6 ms^{-1} are simulated primarily south of the Nile Delta, in the northwestern bay of the Red Sea, and in the northwestern part of the Nafud Desert. Owing to the cooling influence of the sea breeze, land on the Mediterranean coast and the east coast of the Red Sea warms less than the surrounding area around midday and in the evening. As a result, the land–sea temperature gradients hardly changed, and the Mediterranean Sea breeze retained its intensity, whereas the Red Sea breeze was expected to decrease at 1200 UTC.

3.3 Projection of potential wind energy

To determine possible areas that could increase or decrease their potential for generating wind energy due to global warming, the development of potential wind energy (Fig. 6) is compared between the periods 1981–2010 and 2041–2070. The wind at a turbine height of 150 m, which was used to calculate the potential energy, is shown in Fig. 7 in the appendix.

At all times of the day, the highest median potential wind energy of up to 70 GJ(Fig. 6a, d, g, j) is simulated over the northern Red Sea. For most of the day, the regions south of the Nile Delta, east Jordan, the vicinity of the Golan Heights and the Houran Mountains prove to be suitable regions for generating wind energy, reaching values of potential wind energy of approximately 35 GJ(Fig. 6a, d, g, j). The CORDEX-4 simulations by Chen et al. (2018) revealed that the region around the Dead Sea in Jordan and the vicinity of the Judean Mountains have exceptionally high potential for generating wind energy in summer. In contrast, Kiriakidis et al. (2024) computed by WRF-Chem yielded the highest annual average values of potential wind energy in the Houran region, as well as in northern Syria and the northwestern coastal area of the Red Sea. At 0000 UTC, potential energy values below 15 GJ are

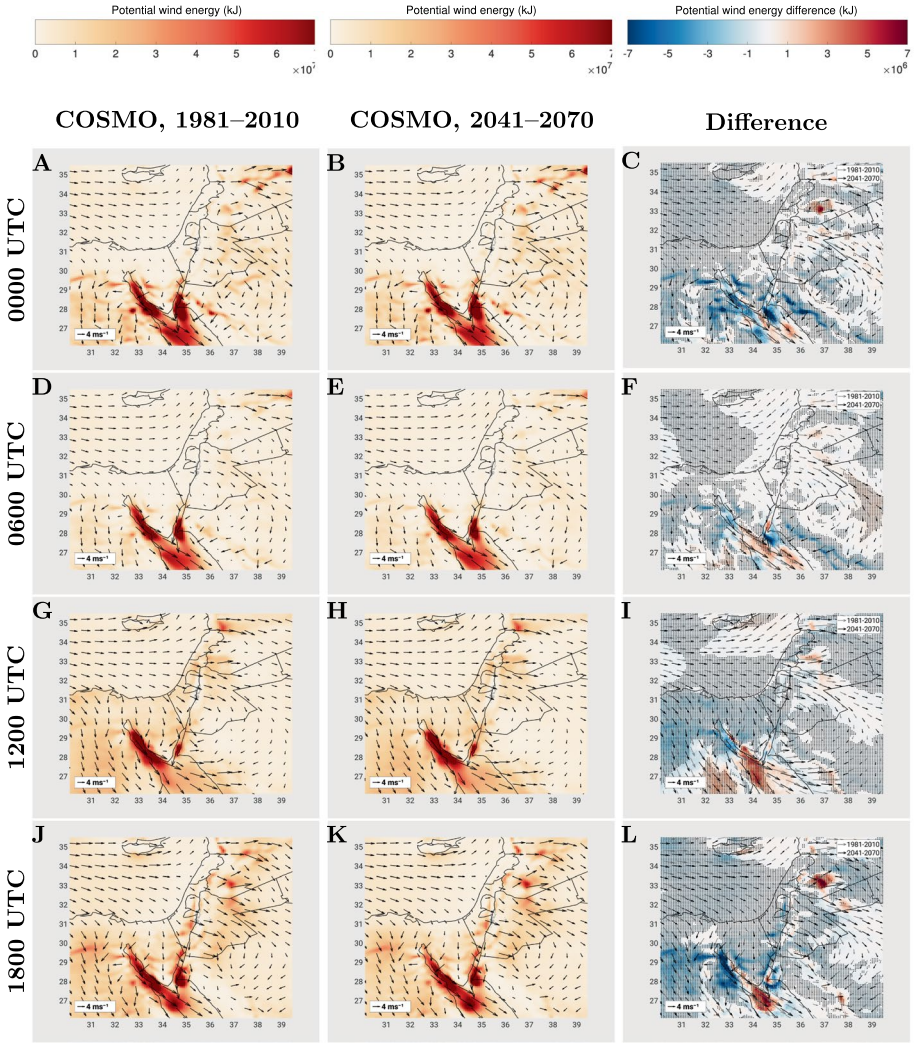

Fig. 6 The same as in Fig. 4, but the colors represent potential wind energy at a height of 150 m for six hours

simulated near the Mediterranean coast, in the Dead Sea valley, and on the east coast of the Red Sea (Fig. 6a, b).

In contrast to the near-surface wind, a significant decrease in the median potential wind energy is simulated for most parts of the simulation area for most of the day. At 0000 UTC, there was a decline in potential wind energy over large areas of the Mediterranean Sea, Egypt, north of the Red Sea, and around the Red Sea, as well as in some regions east of the Mediterranean Sea (Fig. 6c). Particularly large decreases in median potential wind energy of up to 7 GJ within 6 hours are expected in the mountainous regions around the northern Red Sea and in regions over the Eastern Mediterranean (Fig. 6c). The only significant increases in potential wind energy are shown over small areas of the Red Sea and east of the Golan

heights, with values of 2 GJ to 6 GJ. Over the Red Sea, the potential for wind energy is already high, with values between 20 GJ and 70 GJ, making this area particularly suitable for the generation of wind energy.

At 0600 UTC, the median potential energy values are reduced by approximately 30 %(Fig. 6d, e, f) in high-energy regions such as the Red Sea, Nile Delta or southern Syria by 1 ms^{-1} to 2 ms^{-1}. The regions where a decline in wind energy is projected constitute the majority. Over a large part of the Mediterranean, in the Nile Delta, around the Red Sea, and in the area of the Syrian desert, the potential wind energy decreases from 1 GJ to 4 GJ are no longer as high as at 0000 UTC, but the absolute potential wind energy from 1981 to 2010 is also lower at 0600 UTC than at 0000 UTC (Fig. 6f).

At 1200 UTC, despite the increase in near-surface winds, the potential wind energy is projected to decrease in intensity in many regions until 2070 due to climate change (Fig. 7i). The median potential wind energy decreases to 3 GJ within 6 hours over large parts of the Mediterranean, in the Nile Valley, on the Sinai Peninsula, in the northwestern Nafud Desert, and in the Syrian Desert. The 150 m wind speed changes causing wind energy loss may be attributed to changes in the frequency and intensity of the Persian Trough due to climate change, which influences large-scale circulation (Wedler et al. 2023). In addition, the poleward shift of the jet (Eichelberger et al. 2008) and effects such as the stability of the atmosphere and boundary layer height play important roles in the change in wind speed at higher levels (Kim 2022). Additionally, decreasing air density due to higher temperatures can reduce wind energy production. An increase in potential wind energy is limited to the region above the Red Sea, west of the Red Sea, east of Cyprus, and east of the Golan Heights. These regions could benefit from gains of up to 5 GJ in median potential wind energy.

In the evening, the distribution of potential wind energy shifts further inland. In the Red Sea and Mediterranean coastal areas, potential wind energy is already decreasing as the sea wind circulation has lost intensity. By the end of 2070, COSMO simulates significant decreases in potential wind energy (Fig. 7l) in the simulation area at 1800 UTC. The greatest decreases of up to 6 GJ within 6 hours in potential wind energy are predicted in areas over the Mediterranean, south of the Nile delta, in coastal areas of the Red Sea, in the Judean Mountains, and in the Syrian desert. Apart from small, localized increases, a significant increase of up to 7 GJ in potential wind energy is shown only over parts of the Red Sea and east of the Golan heights.

While regionally significant increases up to 0.7 ms^{-1} in the median near-surface wind speed are expected, COSMO simulates an exhaustive decrease regionally up to 7 GJ in the median potential wind energy at most times of the day until 2070 due to climate change. On average, the potential wind energy is projected to decline by 1 GJ. Additionally, its standard deviation is expected to decrease with global warming until 2070 (Table 2). However, the changes in potential wind energy up to 2070 are very heterogeneous and variable. Nevertheless, multiple studies agree that climate change will likely reduce potential wind energy in the eastern Mediterranean. For example, Bloom et al. (2008) investigated the influence of climate change on the development of potential wind energy up to the year 2100 via the regional climate model PRECIS with the IPCC A2 emissions scenario. They project a decrease in expected wind energy for our study area during summer. The decrease over the Mediterranean, Red Sea, and west of the Red Sea is simulated to be exceptionally high, with a reduction of approximately 20%. According to Alvarez and Lorenzo (2019), a decline in

potential wind energy is also simulated in the summer months over the Eastern Mediterranean by 2080 under RCP 4.5, employing wind simulations from the EURO-CORDEX project.

The differing wind patterns near the surface and at 150 m height highlight the need to simulate and evaluate both levels, especially the latter, which corresponds to the wind turbine height, for an accurate assessment of the wind energy potential. Owing to the complex interaction of thermal near-surface wind systems and large-scale synoptic circulation, wind speed can develop differently near the ground than at higher altitudes. To date, the Red Sea, the Judean Mountains, the Nile Delta, the Sinai Peninsula, and the plain in Saudi Arabia have high potential for wind energy, with medians of over 3.8 GJ within 6 hours (Table 2). The Red Sea stands out in particular, with a median of 27.4 GJ(Table 2). An increase in the median of 801 kJ is projected there, and a decrease in the standard deviation of 3539 kJ is projected. In addition to the Red Sea, the Saudi Arabian Plain is the only area where a slight increase of 117 kJ in the median potential wind energy is expected. COSMO simulates a decline in potential wind energy for the Mediterranean and all other inland regions. It is therefore predicted that the Red Sea area, the Sinai Peninsula, the plain in Saudi Arabia, and the Judean Mountains will continue to be particularly suitable for generating wind energy in the Eastern Mediterranean region until 2070 (Tables 1 and 2).

4 Summary and conclusions

Our study offers detailed insights into the relationships among climate change, wind patterns, and wind energy potential in the Middle East and their implications for future energy planning and resource management (Sayed et al. 2021). By utilizing the COSMO-CLM regional climate model with 8 km grid spacing, we thoroughly analyzed summer wind patterns across the region, allowing for an in-depth exploration of regional climate dynamics. While our research confirms the overall effectiveness of the COSMO-CLM model in capturing broad-scale wind patterns in the Middle East, it also highlights significant uncertainties, especially in coastal and mountainous areas. These findings emphasize the need for further research and coordinated efforts to improve our understanding and modeling of smaller-

Table 1 Mean, median, and standard deviation for near-surface and 150 m (in brackets) wind speeds in ms^{-1} for the periods 1981–2010 and 2041–2070

Subarea	Mean		Median		Standard deviation	
	1981-2010	2041-2070	1981-2010	2041-2070	1981-2010	2041-2070
Golan Heights	3.68 (4.74)	3.66 (4.61)	3.16 (4.44)	3.19 (4.33)	2.42 (2.85)	2.35 (2.70)
Red Sea	7.30 (9.80)	7.35 (9.86)	7.32 (10.22)	7.40 (10.32)	3.78 (4.70)	3.78 (4.49)
Mediterranean Sea	4.10 (4.96)	4.06 (4.71)	3.68 (4.61)	3.69 (4.42)	2.27 (2.56)	2.18 (2.33)
Judean Mountains	4.24 (5.61)	4.21 (5.47)	3.90 (5.42)	3.91 (5.28)	2.26 (2.81)	2.19 (2.70)
Peninsula Sinai	4.84 (6.46)	4.83 (6.25)	4.80 (6.53)	4.81 (6.34)	2.38 (3.28)	2.35 (3.14)
Nile Delta	4.46 (6.38)	4.49 (5.25)	4.20 (5.31)	4.25 (5.09)	2.08 (2.29)	2.04 (2.21)
Red Sea east coast	4.05 (5.22)	3.96 (4.93)	3.45 (4.66)	3.35 (4.34)	2.69 (3.54)	2.65 (3.37)
Plain	4.70 (5.85)	4.78 (5.87)	4.60 (5.81)	4.71 (5.85)	2.04 (2.55)	1.99 (2.42)
Mediterranean Sea east coast	3.16 (3.69)	3.13 (3.68)	2.59 (3.25)	2.59 (3.11)	2.15 (2.53)	2.09 (2.43)
Average	4.64 (5.87)	4.62 (5.64)	4.08 (5.17)	4.09 (4.98)	2.79 (3.48)	2.75 (3.38)

Table 2 Mean, median, and standard deviation for 150 m potential wind energy in *kJ* within 6 hours for the periods 1981–2010 and 2041–2070

Subarea	Mean		Median		Standard deviation	
	1981-2010	2041-2070	1981-2010	2041-2070	1981-2010	2041-2070
Golan Heights	6054	5385	2246	2075	10290	8759
Red Sea	40584	39496	27362	28163	44028	40489
Mediterranean Sea	5973	4941	2518	2212	10262	8476
Judean Mountains	8149	7452	4081	3779	11251	10107
Peninsula Sinai	12468	11143	7138	6530	16660	14752
Nile Delta	6381	5748	3831	3388	7183	6461
Red Sea east coast	9585	8216	2591	2095	18519	16163
Plain	8140	7890	5015	5132	9570	8853
Mediterranean Sea east coast	3688	3255	882	770	7528	6387
Average	11609	10637	3533	3159	22901	21239

scale processes affecting wind variability in these complex terrains. Employing multi model approaches could be beneficial in reducing these uncertainties (Pryor et al. 2020). A pivotal finding of our investigation, although based on one single model result, is the significant regional increase of up to $0.7\,\mathrm{ms}^{-1}$ in median surface wind speeds observed across the Middle East, driven primarily by enhanced land–sea temperature contrasts; this can moderate some of the increasing heat stress caused by climate change. Conversely, at the 150-m wind turbine height, we observed substantial decreases of up to $1.0\,\mathrm{ms}^{-1}$ in the median wind speed, attributed to changes in the frequency and intensity of the Persian Trough synoptic system (Hochman et al. 2018c; Wedler et al. 2023). Another reason for the decrease in 150 m wind speeds could be the polar amplification of global warming; this leads to a significant decrease in the meridional temperature gradient, which may weaken the jet stream and change its location (Martinez and Iglesias 2024). Regionally, this implies decreases in median potential wind energy up to 7 GJ within six hours. This underscores the importance of considering both surface and upper-level wind characteristics when assessing the impacts of climate change on wind energy resources, particularly in regions where upper-level wind dynamics play a significant role (Hochman et al. 2023). Moreover, our analysis revealed a spatially heterogeneous pattern of changes in the wind energy potential across the region. While decreases were evident over much of the Middle East, particularly in inland areas and over the Mediterranean Sea, some regions, notably the Red Sea, presented increases in wind energy potential. These spatial variations emphasize the need for tailored strategies to harness wind energy resources effectively, considering local climatic and geographic factors, including offshore wind turbines (Costoya et al. 2021; Li et al. 2020; Akhtar et al. 2021). As a caveat, although we analyzed a computationally expensive, long-term, high-resolution simulation, it is indeed a single-model simulation, affected by uncertainties such as the choice of the global circulation model, the representative concentration pathway scenario, the nesting strategies, and the setup. These uncertainties are not considered here and must be addressed in follow-up studies. In conclusion, the findings of this study provide valuable guidance for policy-makers and energy planners seeking to develop sustainable energy strategies and optimize the utilization of wind energy resources in the region. Further research efforts are warranted to refine the understanding of regional wind dynamics and inform evidence-based decision-making regarding climate change adaptation and mitigation strategies.

Appendix

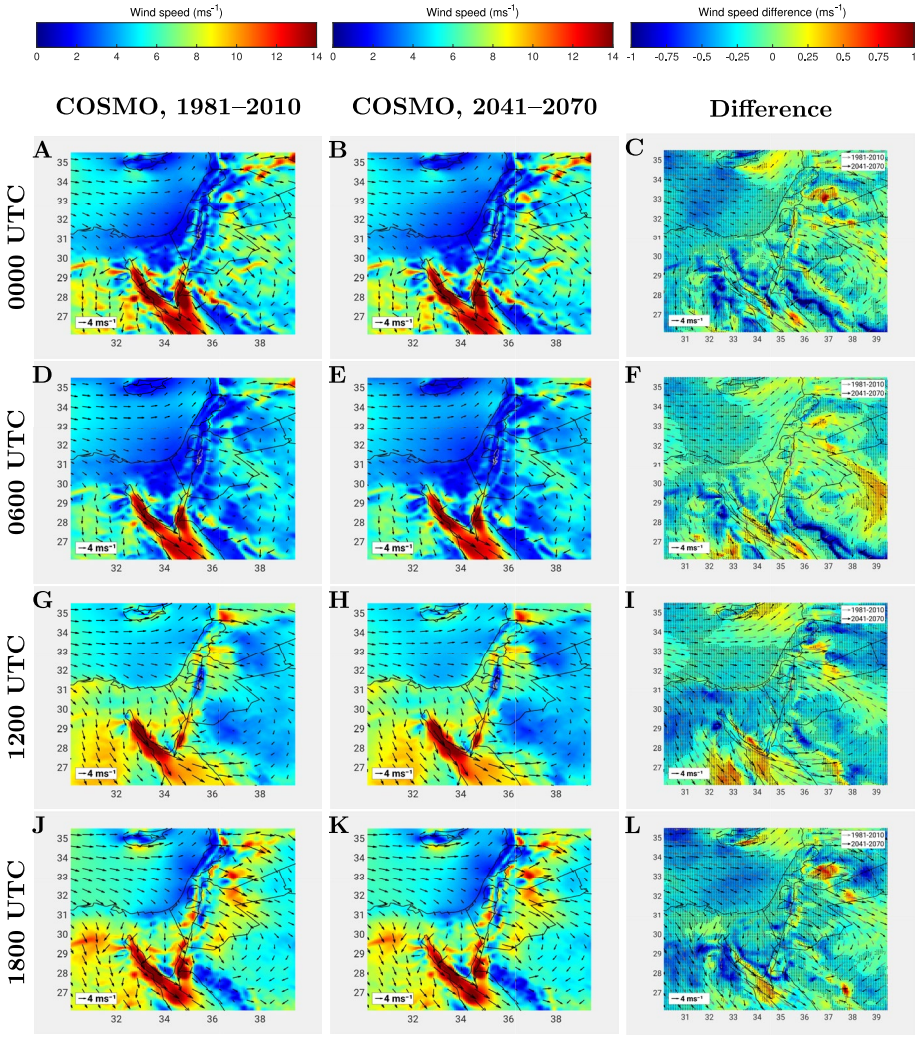

Fig. 7 The same as Fig. 4 but for wind in 150 m height

Acknowledgements The Israel Science Foundation (grant #978/23), the Planning and Budgeting Committee of the Israeli Council for Higher Education under the 'MedWORLD' Consortium, and the COST Action CA22162 - FutureMed: A Transdisciplinary Network to Bridge Climate Science and Impacts on Society (FutureMed) supported by COST (European Cooperation in Science and Technology) fund AH's contribution. M. R. Latt thanks the German Helmholtz Association (Changing Earth program) for funding. M. A. and P.M. acknowledge the regional climate COSMO model in CLimate Mode (COSMO-CLM) and the German regional climate research team that, jointly with the CLM-Community, further developed the model. The CMCC simulations were performed via CMCC Supercomputing Centre facilities. Finally, we acknowledge the use of Grammarly for grammar and spell checks.

Author Contributions Melissa Latt: Conceptualization, Formal analysis, Investigation, Writing - Original Draft, Writing - Review and Editing, Visualization. Marianna Adinolfi: Methodology, Validation, Investigation, Resources, Writing - Original Draft, Writing - Review and Editing. Paola Mercogliano: Methodology, Validation, Investigation, Resources, Writing - Review and Editing. Assaf Hochman: Conceptualization, Investigation, Writing - Original Draft, Writing - Review and Editing, Supervision, Funding acquisition.

Funding Open Access funding enabled and organized by Projekt DEAL.

Data Availability The data are available upon request to the authors.

Declarations

Competing Interests The authors have no relevant financial or non-financial interests to disclose.

References

Adekoya L, Adewale A (1992) Wind energy potential of Nigeria. Renew Energy 2(1):35–39
Adinolfi M, Rianna G, Mercogliano P et al (2020) Behaviour of energy piles under climate-change scenarios: a case study in Southern Italy. Environ Geotech 8(8):571–585
Adinolfi M, Raffa M, Reder A et al (2023) Investigation on potential and limitations of era5 reanalysis downscaled on Italy by a convection-permitting model. Clim Dyn 61(9):4319–4342
Akhtar N, Geyer B, Rockel B et al (2021) Accelerating deployment of offshore wind energy alter wind climate and reduce future power generation potentials. Sci Rep 11(1):11826
Alpert P, Getenio B (1988) One-level diagnostic modeling of mesoscale surface winds in complex terrain. Part i: Comparison with three-dimensional modeling in Israel. Mon Weather Rev 116(10):2025–2046
Alpert P, Abramsky R, Neeman BU (1990) The prevailing summer synoptic system in Israel—subtropical high, not Persian trough. Isr J Earth Sci 39(2–4):93–102
Alpert P, Osetinsky I, Ziv B et al (2004a) A new seasons definition based on classified daily synoptic systems: an example for the Eastern Mediterranean. Int J Climatol J R Meteorol Soc 24(8):1013–1021
Alpert P, Osetinsky I, Ziv B et al (2004b) Semi-objective classification for daily synoptic systems: application to the eastern Mediterranean climate change. Int J Climatol J R Meteorol Soc 24(8):1001–1011
Alvarez I, Lorenzo MN (2019) Changes in offshore wind power potential over the Mediterranean sea using cordex projections. Reg Environ Chang 19:79–88
Amran YA, Amran YM, Alyousef R et al (2020) Renewable and sustainable energy production in Saudi Arabia according to Saudi vision 2030; current status and future prospects. J Clean Prod 247:119602
Åström DO, Bertil F, Joacim R (2011) Heat wave impact on morbidity and mortality in the elderly population: a review of recent studies. Maturitas 69(2):99–105
Baltaci H (2021) Meteorological characteristics of dust storm events in turkey. Aeolian Res 50:100673
Bloom A, Kotroni V, Lagouvardos K (2008) Climate change impact of wind energy availability in the Eastern Mediterranean using the regional climate model precis. Nat Hazards Earth Syst Sci 8(6):1249–1257
Bucchignani E, Mercogliano P, Panitz HJ et al (2018) Climate change projections for the Middle East-North Africa domain with cosmo-clm at different spatial resolutions. Adv Clim Chang Res 9(1):66–80
Bucchignani E, Cattaneo L, Panitz HJ et al (2016a) Sensitivity analysis with the regional climate model cosmo-clm over the cordex-mena domain. Meteorog Atmos Phys 128:73–95
Bucchignani E, Mercogliano P, Rianna G et al (2016b) Analysis of era-interim-driven cosmo-clm simulations over Middle East-North Africa domain at different spatial resolutions. Int J Climatol 36(9):3346–3369
Chen K, Bi J, Chen J et al (2015) Influence of heat wave definitions to the added effect of heat waves on daily mortality in Nanjing, China. Sci Total Environ 506:18–25

Chen W, Castruccio S, Genton MG et al (2018) Current and future estimates of wind energy potential over Saudi Arabia. J Geophys Res: Atmospheres 123(12):6443–6459
Copernicus Climate Change Service CDS (2019) Uerra regional reanalysis for europe on single levels from 1961 to 2019. https://doi.org/10.24381/cds.32b04ec5. Accessed Dec 2023
Costoya X, DeCastro M, Carvalho D et al (2021) Climate change impacts on the future offshore wind energy resource in China. Renew Energy 175:731–747
Crouvi O, Dayan U, Amit R et al (2017) An Israeli haboob: sea breeze activating local anthropogenic dust sources in the Negev loess. Aeolian Res 24:39–52
Dee DP, Uppala SM, Simmons AJ et al (2011) The era-interim reanalysis: configuration and performance of the data assimilation system. Q J R Meteorol Soc 137(656):553–597
Eichelberger S, McCaa J, Nijssen B et al (2008) Climate change effects on wind speed. N Am Windpower 7:68–72
Eitan A, Fischhendler I (2023) The architecture of inter-community partnerships in renewable energy: the role of climate intermediaries. Policy Stud 44(5):572–588
El-Geziry TM, Elbessa M, Tonbol KM (2021) Climatology of sea-land breezes along the Southern Coast of the Levantine Basin. Pure Appl Geophys 178(5):1927–1941
Evans JP (2009) 21st century climate change in the Middle East. Clim Change 92(3):417–432
Gasch P, Rieger D, Walter C et al (2017) Revealing the meteorological drivers of the September 2015 severe dust event in the Eastern Mediterranean. Atmos Chem Phys 17(22):13573–13604
Gernaat DE, de Boer HS, Daioglou V et al (2021) Climate change impacts on renewable energy supply. Nat Clim Change 11(2):119–125
Giorgi F, Gutowski WJ Jr (2015) Regional dynamical downscaling and the cordex initiative. Annu Rev Environ Resour 40:467–490
Giorgi F, Lionello P (2008) Climate change projections for the Mediterranean region. Global Planet Chang 63(2–3):90–104
Giorgi F, Jones C, Asrar GR et al (2009) Addressing climate information needs at the regional level: the cordex framework. World Meteorol Organ (WMO) Bull 58(3):175
Hamdi M, Ragab R, El Salmawy HA (2023) The value of diurnal and seasonal energy storage in baseload renewable energy systems: a case study of ras Ghareb-Egypt. J Energy Storage 61:106764
Harpaz T, Ziv B, Saaroni H et al (2014) Extreme summer temperatures in the East Mediterranean—dynamical analysis. Int J Climatol 34(3):849–862
Hassan Q, Al-Hitmi M, Tabar VS et al (2023) Middle East energy consumption and potential renewable sources: an overview. Clean Eng Technol 12:100599
Hochman A, Scher S, Quinting J et al (2021) A new view of heat wave dynamics and predictability over the Eastern Mediterranean. Earth Syst Dyn 12(1):133–149
Hochman A, Marra F, Messori G et al (2022) Extreme weather and societal impacts in the Eastern Mediterranean. Earth Syst Dyn 13(2):749–777
Hochman A, Komacek TD, De Luca P (2023) Analogous response of temperate terrestrial exoplanets and earth's climate dynamics to greenhouse gas supplement. Sci Rep 13(1):11123
Hochman A, Bucchignani E, Gershtein G et al (2018a) Evaluation of regional cosmo-clm climate simulations over the Eastern Mediterranean for the period 1979–2011. Int J Climatol 38(3):1161–1176
Hochman A, Harpaz T, Saaroni H et al (2018b) The seasons' length in 21st century cmip5 projections over the Eastern Mediterranean. Int J Climatol 38(6):2627–2637
Hochman A, Harpaz T, Saaroni H et al (2018c) Synoptic classification in 21st century cmip5 predictions over the eastern Mediterranean with focus on cyclones. Int J Climatol 38(3):1476–1483
Holtz G, Fink T (2015) Analysing the transition of jordan's electricity system: underpinning transition pathways with mechanisms. 6th International sustainability transitions conference 2015, Brighton
Iglesias J, Cuesta I, Salueña C et al (2023) Analysis and comparison of coupled and uncoupled simulations with the coawst model during the gloria storm (January 2020) in the northwestern Mediterranean sea. Environ Model Softw 169:105830
Imam AA, Abusorrah A, Marzband M (2024) Potentials and opportunities of solar pv and wind energy sources in Saudi Arabia: land suitability, techno-socio-economic feasibility, and future variability. Results Eng
Jung C, Schindler D (2022) A review of recent studies on wind resource projections under climate change. Renew Sustain Energy Rev 165:112596
Kaiser-Weiss AK, Borsche M, Niermann D et al (2019) Added value of regional reanalyses for climatological applications. Environ Res Commun 1(7):071004
Katal F, Fazelpour F (2018) Multi-criteria evaluation and priority analysis of different types of existing power plants in Iran: an optimized energy planning system. Renew Energy 120:163–177
Kharat Halou M (2012) Wind power business in the Middle East and North Africa. Masters Thesis in Economics and Business Administration

Kim KY (2022) Diurnal and seasonal variation of planetary boundary layer height over East Asia and its climatic change as seen in the era-5 reanalysis data. SN Appl Sci 4(2):39
Kiriakidis P, Christoudias T, Kushta J et al (2024) Projected wind and solar energy potential in the Eastern Mediterranean and Middle East in 2050. Sci Total Environ 172120
Kishcha P, Starobinets B, Alpert P (2018) Modeling of foehn-induced extreme local dust pollution in the dead sea valley. In: Air pollution modeling and its application XXV 35. Springer, pp 433–437
Krichak SO, Alpert P, Kunin P (2010) Numerical simulation of seasonal distribution of precipitation over the Eastern Mediterranean with a rcm. Clim Dyn 34:47–59
Kulkarni S, Deo M, Ghosh S (2019) Performance of the cordex regional climate models in simulating offshore wind and wind potential. Theor Appl Climatol 135:1449–1464
Kunin P, Alpert P, Rostkier-Edelstein D (2019) Investigation of sea-breeze/foehn in the dead sea valley employing high resolution wrf and observations. Atmos Res 229:240–254
Langodan S, Cavaleri L, Vishwanadhapalli Y et al (2017) The climatology of the red sea-part 1: the wind. Int J Climatol 37(13):4509–4517
Latt MR, Hochman A, Caldas-Alvarez A et al (2022) Understanding summer wind systems over the Eastern Mediterranean in a high-resolution climate simulation. Int J Climatol 42(15):8112–8131
Lawrence PJ, Chase TN (2007) Representing a new modis consistent land surface in the community land model (clm 3.0). J Geophys Res: Biogeosciences 112(G1)
Lee S, Lee H, Myung W et al (2018) Mental disease-related emergency admissions attributable to hot temperatures. Sci Total Environ 616:688–694
Lelieveld J, Hadjinicolaou P, Kostopoulou E et al (2014) Model projected heat extremes and air pollution in the Eastern Mediterranean and Middle East in the twenty-first century. Reg Environ Change 14:1937–1949
Li J, Wang G, Li Z et al (2020) A review on development of offshore wind energy conversion system. Int J Energy Res 44(12):9283–9297
Martinez A, Iglesias G (2024) Global wind energy resources decline under climate change. Energy 288:129765
Molina MO, Careto J, Gutiérrez C et al (2024) The added value of simulated near-surface wind speed over the alps from a km-scale multimodel ensemble. Clim Dyn 1–19
Moss RH, Edmonds JA, Hibbard KA et al (2010) The next generation of scenarios for climate change research and assessment. Nature 463(7282):747–756
Muñoz Sabater J (2019) Era5-land hourly data from 1950 to present. https://doi.org/10.24381/cds.e2161bac. Accessed Feb 2022
Muñoz-Sabater J, Dutra E, Agustí-Panareda A et al (2021) Era5-land: a state-of-the-art global reanalysis dataset for land applications. Earth Syst Sci Data 13(9):4349–4383
Naor R, Potchter O, Shafir H et al (2017) An observational study of the summer Mediterranean sea breeze front penetration into the complex topography of the Jordan Rift Valley. Theor Appl Climatol 127:275–284
Nolan P, Lynch P, Sweeney C (2014) Simulating the future wind energy resource of Ireland using the cosmo-clm model. Wind Energy 17(1):19–37
Pryor SC, Barthelmie RJ, Bukovsky MS et al (2020) Climate change impacts on wind power generation. Nat Rev Earth Environ 1(12):627–643
Reale M, Cabos Narvaez WD, Cavicchia L et al (2022) Future projections of Mediterranean cyclone characteristics using the med-cordex ensemble of coupled regional climate system models. Clim Dyn 1–24
Rezazadeh M, Irannejad P, Shao Y (2013) Climatology of the Middle East dust events. Aeolian Res 10:103–109
Rockel B, Will A, Hense A (2008) The regional climate model cosmo-clm (cclm). Meteorol Z 17(4):347
Saaroni H, Savir A, Ziv B (2017) Synoptic classification of the summer season for the levant using an 'environment to climate'approach. Int J Climatol 37(13):4684–4699
Sadorsky P (2021) Wind energy for sustainable development: driving factors and future outlook. J Clean Prod 289:125779
Samuels R, Hochman A, Baharad A et al (2018) Evaluation and projection of extreme precipitation indices in the Eastern Mediterranean based on cmip5 multi-model ensemble. Int J Climatol 38(5):2280–2297
Sayed ET, Wilberforce T, Elsaid K et al (2021) A critical review on environmental impacts of renewable energy systems and mitigation strategies: wind, hydro, biomass and geothermal. Sci Total Environ 766:144505
Scoccimarro E, Gualdi S, Bellucci A et al (2011) Effects of tropical cyclones on ocean heat transport in a high-resolution coupled general circulation model. J Clim 24(16):4368–4384
Serckx A, Pollard E, Wilson D et al (2018) Lekela North Ras Gharib 250 mw project: critical habitat assessment
Shafir H, Jin F, Lati Y et al (2008) Wind channeling by the dead-sea wadis. Open Atmos Sci J 2(1)

Steppeler J, Doms G, Schättler U et al (2003) Meso-gamma scale forecasts using the nonhydrostatic model lm. Meteorol Atmos Phys 82:75–96
Tapiador FJ, Navarro A, Moreno R et al (2020) Regional climate models: 30 years of dynamical downscaling. Atmos Res 235:104785
Tegen I, Hollrig P, Chin M et al (1997) Contribution of different aerosol species to the global aerosol extinction optical thickness: estimates from model results. J Geophys Res 102(23):895–23
Tiedtke M (1989) A comprehensive mass flux scheme for cumulus parameterization in large-scale models. Mon Weather Rev 117(8):1779–1800
Uppala SM, Kållberg P, Simmons AJ et al (2005) The era-40 re-analysis. Q J R Meteorol Soc J Atmos Sci Appl Meteorol Phys Oceanogr 131(612):2961–3012
Wedler M, Pinto JG, Hochman A (2023) More frequent, persistent, and deadly heat waves in the 21st century over the Eastern Mediterranean. Sci Total Environ 870:161883
Wilcoxon F, Katti S, Wilcox RA et al (1970) Critical values and probability levels for the Wilcoxon rank sum test and the Wilcoxon signed rank test. Sel Tables Math Stat 1:171–259
Zittis G, Hadjinicolaou P, Fnais M et al (2016) Projected changes in heat wave characteristics in the Eastern Mediterranean and the Middle East. Reg Environ Chang 16:1863–1876
Zittis G, Almazroui M, Alpert P et al (2022) Climate change and weather extremes in the Eastern Mediterranean and Middle East. Rev Geophys 60(3):e2021RG000762
Ziv B, Saaroni H, Alpert P (2004) The factors governing the summer regime of the Eastern Mediterranean. Int J Climatol J R Meteorol Soc 24(14):1859–1871

Authors and Affiliations

Melissa Latt[1] · Marianna Adinolfi[2] · Paola Mercogliano[2] · Assaf Hochman[3]

✉ Melissa Latt
melissa.latt@kit.edu

✉ Assaf Hochman
Assaf.Hochman@mail.huji.ac.il

Marianna Adinolfi
marianna.adinolfi@cmcc.it

Paola Mercogliano
paola.mercogliano@cmcc.it

[1] Institute of Meteorology and Climate Research (IMKTRO), Karlsruhe Institute of Technology (KIT), Karlsruhe, Germany

[2] CMCC Foundation - Euro-Mediterranean Center on Climate Change, Lecce, Italy

[3] Fredy and Nadine Herrmann Institute of Earth Sciences, The Hebrew University of Jerusalem, Jerusalem, Israel